

# Origin of Size Dependency in Coherent-Twin-Propagation-Mediated Tensile Deformation of Noble Metal Nanowires

Jong-Hyun Seo,<sup>†,‡,∇</sup> Harold S. Park,<sup>§,∇</sup> Youngdong Yoo,<sup>||</sup> Tae-Yeon Seong,<sup>‡</sup> Ju Li,<sup>⊥,||</sup> Jae-Pyoung Ahn,<sup>\*,†</sup> Bongsoo Kim,<sup>\*,||</sup> and In-Suk Choi<sup>\*,#</sup>

<sup>†</sup>Advanced Analysis Center, KIST, Seoul 136-791, Korea

<sup>‡</sup>Department of Materials Science and Engineering, Korea University, Seoul 136-701, Korea

<sup>§</sup>Department of Mechanical Engineering, Boston University, Boston, Massachusetts 02215, United States

<sup>||</sup>Department of Chemistry, KAIST, Daejeon 305-701, Korea

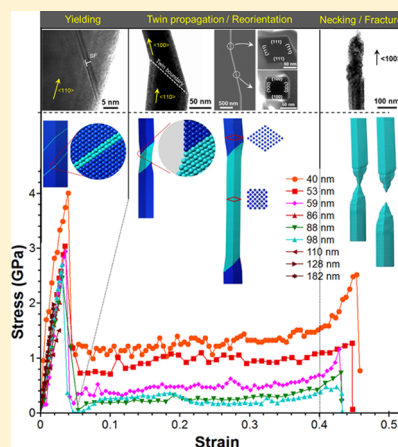
<sup>⊥</sup>Department of Nuclear Science and Engineering and <sup>||</sup>Department of Materials Science and Engineering, Massachusetts Institute of Technology, Cambridge, Massachusetts 02139, United States

<sup>#</sup>High Temperature Energy Materials Research Center, KIST, Seoul 136-791, Korea

## S Supporting Information

**ABSTRACT:** Researchers have recently discovered ultrastrong and ductile behavior of Au nanowires (NWs) through long-ranged coherent-twin-propagation. An elusive but fundamentally important question arises whether the size and surface effects impact the twin propagation behavior with a decreasing diameter. In this work, we demonstrate size-dependent strength behavior of ultrastrong and ductile metallic NWs. For Au, Pd, and AuPd NWs, high ductility of about 50% is observed through coherent twin propagation, which occurs by a concurrent reorientation of the bounding surfaces from {111} to {100}. Importantly, the ductility is not reduced with an increase in strength, while the twin propagation stress dramatically increases with decreasing NW diameter from 250 to 40 nm. Furthermore, we find that the power-law exponent describing the twin propagation stress is fundamentally different from the exponent describing the size-dependence of the yield strength. Specifically, the inverse diameter-dependence of the twin propagation stress is directly attributed to surface reorientation, which can be captured by a surface energy differential model. Our work further highlights the fundamental role that surface reorientations play in enhancing the size-dependent mechanical behavior and properties of metal NWs that imply the feasibility of high efficiency mechanical energy storage devices suggested before.

**KEYWORDS:** Nanowires, ultrastrong and ductile, twin propagation, size effect, surface energy



The question of how the mechanical properties of metallic materials change as their characteristic sizes are reduced to nanometer dimensions has recently attracted significant scientific interest.<sup>1–3</sup> In an attempt to answer this fundamental question, the mechanical behavior of single crystalline metal nanowires (NWs) under tensile loading has been extensively studied primarily using classical molecular dynamics,<sup>1,4</sup> and many resulting predictions of unique mechanical behavior emerges specifically as a result of the nanometer dimensionality.

Experimental investigation into this question has also been explored through recent advances in the synthesis of dislocation-free, single-crystalline metal NWs.<sup>5–7</sup> However, due to a range of experimental difficulties related to manipulating and applying loads to nanosized objects, there have been comparably few experimental reports on the tensile stress-induced plastic deformation of metal NWs.<sup>5,8–13</sup> While most of previous experimental studies found that metal NWs exhibit very high strength,<sup>5,9,11–14</sup> they also observed that the subsequent failure of the NWs was almost always brittle,

typically with fracture strains less than 5%,<sup>5,14</sup> and some reporting fracture strains in the 10–15% range.<sup>11–13</sup> In contrast, a recent study from our group reported unique and highly desirable combination of ultrastrong and ductile behavior of Au NWs with fracture strains near 50% through twin propagation,<sup>9</sup> as was predicted by classical molecular dynamics for other face-centered cubic (fcc) metals.<sup>15–19</sup>

Some fundamental questions are still to be resolved. Can we observe size-dependent mechanical properties in these ultrastrong and ductile metallic NWs? Is there any difference in the size-dependent behavior between yielding and twin propagation? Can we conclusively establish a direct connection between concurrent geometric and surface reorientations

**Received:** June 21, 2013

**Revised:** September 8, 2013

**Published:** September 27, 2013

during plastic deformation and the size-dependent mechanical properties under tensile loading for NWs?

In this work, we present answers to these key questions through in situ tensile testing of single crystalline Au, Pd, and AuPd NWs with diameters of 40–250 nm. Interestingly, we find that the size-dependent behavior of twin propagation is different from that of yielding. Furthermore, we theoretically associate the stress required for twin propagation (twin propagation stress) with the surface energy change resulting from the tensile stress-induced reorientation of the NW from  $\{111\}$  to  $\{100\}$ , thereby explaining the experimentally observed inverse proportionality of the twin propagation stress to the NW diameter. We also find that the energetic cost of the surface reorientation becomes important at a critical NW diameter of  $\sim 100$  nm at which point the twin propagation stress increases substantially. Our results unambiguously demonstrate the fundamental role that surface reorientations play in enhancing the size-dependent mechanical behavior and properties of metal NWs and imply the feasibility of high-efficiency mechanical energy storage devices and shape memory application of NWs suggested by a number of theoretical studies.<sup>15–19</sup>

Defect-free single crystalline Au, Pd, and AuPd NWs with diameters ranging from 40 to 250 nm and lengths of 5 to 20  $\mu\text{m}$  were synthesized using the vapor transport method.<sup>6,7</sup> The detailed structural information of the as-grown NWs was given in our previous works,<sup>6,7</sup> where high-resolution TEM (HRTEM) images and selected area electron diffraction (SAED) patterns showed the single crystalline and twin-free nature of the vertically grown NWs. The NWs all have a  $\langle 110 \rangle$  axial growth direction and a rhombic cross-section bounded by four equivalent close-packed  $\{111\}$  transverse surfaces. The in situ tensile tests were carried out in a dual beam electro-microscope (FEI). To apply tensile loading, one end of the NW was fixed to a nanomanipulator (MM3A, Kleindick) tungsten tip and the other end to a silicon cantilever as part of a force measurement system (FMS, Kleindick) by FIB Pt deposition. The NW was subsequently pulled in tension at a displacement rate of  $1.9 \times 10^{-7}$  m/sec (see also Supporting Information Movie S1 and S2).

Ultrastrong and ductile tensile deformation process was clearly observed for Pd and AuPd NWs as well as for Au NWs, consistent with predictions by molecular dynamics (MD) simulations for other fcc metal NWs.<sup>16–18</sup> A representative deformation behavior of the Pd NW is illustrated via the TEM and SEM images and the three-stage stress–strain curve in Figure 1 (see also Supporting Information Movie S1). In the yielding stage (stage 1), the initially rhombic cross section of the  $\langle 110 \rangle$  NW with  $\{111\}$  transverse surfaces ( $\langle 110 \rangle / \{111\}$  NW) deforms elastically until the stress drops because of the nucleation of a twin (the yield stress). The plateau stress–strain region that defines the twin propagation stage (stage 2) appears due to the stress-induced propagation of the twin boundary along the NW length of more than  $1 \mu\text{m}$ . SAED patterns of the original and twinned regions (Supporting Information Figure S1b–d) show that the twin formation reorients the lattice of the NW from  $\langle 110 \rangle$  to  $\langle 100 \rangle$ . The twin propagation results in the reorientation of the initially  $\{111\}$  surfaces to  $\{100\}$  surfaces of a higher energy with a reorientation of the NW cross section changing from rhombic to square, eventually leading to a  $\langle 100 \rangle / \{100\}$  NW after  $\sim 40\%$  tensile strain. The geometric reorientation of the cross section from rhombic to square and the  $\sim 40\%$  tensile strain required to

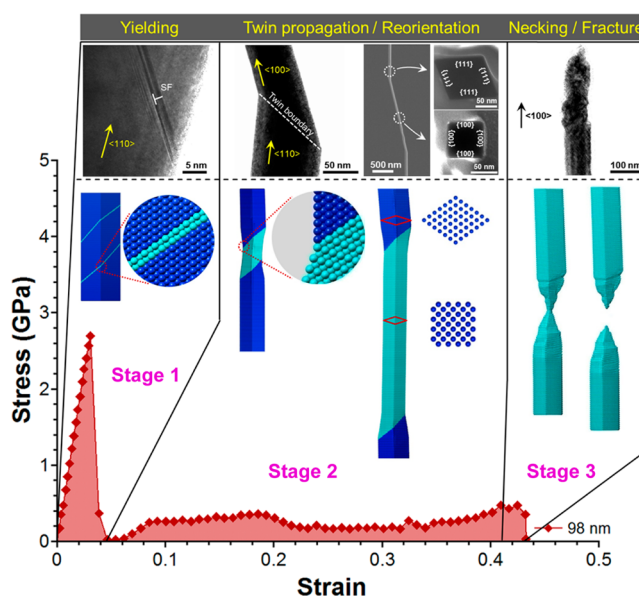
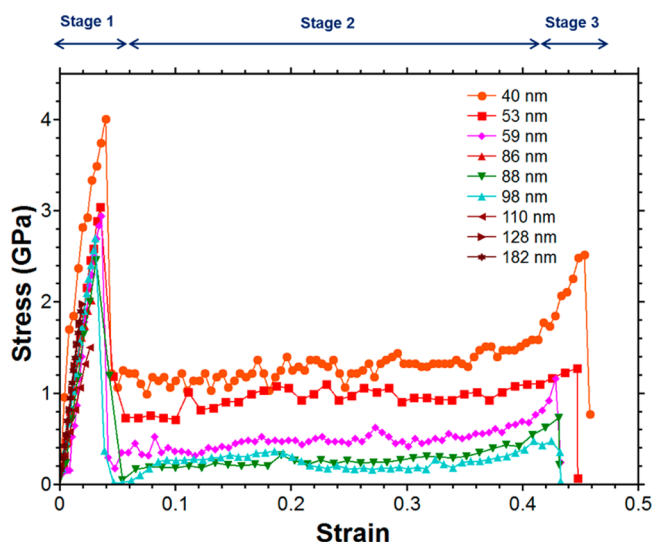


**Figure 1.** Three distinct stages of uniaxial tensile deformation for a representative Pd NW with a diameter of 98 nm. Stage 1: elastic deformation of an initially  $\langle 110 \rangle / \{111\}$  rhombic NW. Nanotwins composed of stacking faults were nucleated upon abrupt load drop as shown in the inset. SF represents stacking faults. Stage 2: twin propagation and concurrent reorientation of the rhombic  $\langle 110 \rangle / \{111\}$  NW to a square  $\langle 100 \rangle / \{100\}$  NW (see Supporting Information Figure S1 for SAED patterns). The long-range order coherent twin propagation results in about 40% elongation. Stage 3: deformation and eventual fracture of a reoriented  $\langle 100 \rangle / \{100\}$  NW (see also Supporting Information Movies S1 and S2).

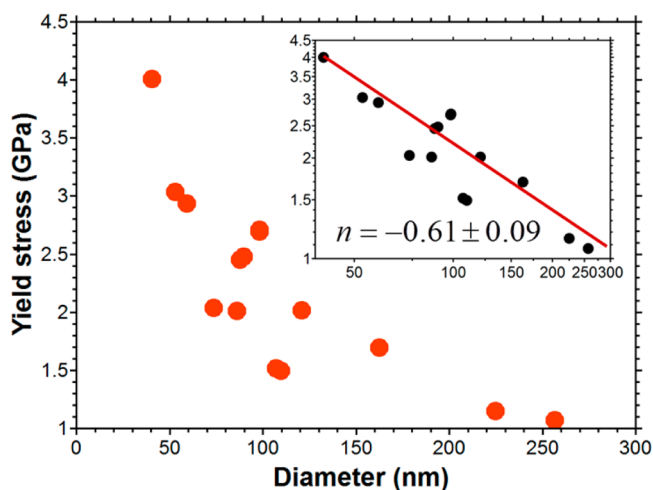
complete the process matches with the 41% strain predicted by MD simulations.<sup>19</sup> This reorientation strain of 41% is also important because it is about 1 order of magnitude longer than observed in conventional bulk shape memory alloys such as NiTi.<sup>20–22</sup> Finally, after the reorientation process is complete linear elastic deformation of the resulting  $\langle 100 \rangle / \{100\}$  NW proceeds during a fracture stage (stage 3). Yield of the reoriented  $\langle 100 \rangle / \{100\}$  NW occurs via the nucleation and propagation of full and partial dislocations, as previously observed in MD simulations and experiment<sup>9,23,24</sup> leading to fracture after about 3.1% strain of the  $\langle 100 \rangle / \{100\}$  NW, and a total of 43.5% strain for the initial  $\langle 110 \rangle / \{111\}$  NW. This fracture strain of nearly 50% demonstrates that these rhombic  $\langle 110 \rangle / \{111\}$  metal NWs are exceptionally ductile.

Figure 2 shows complete stress–strain curves for the  $\langle 110 \rangle / \{111\}$  Pd NWs with diameters of 40–182 nm. Importantly, while twin propagation induced ductility with about 50% strain is observed regardless of the NW diameter, it is clearly seen that there is size-dependence both in the yield stress of the  $\langle 110 \rangle / \{111\}$  NWs and in the twin propagation stress which drives the reorientation of the NW from  $\langle 110 \rangle / \{111\}$  to  $\langle 100 \rangle / \{100\}$ .

We first discuss the size-dependence of the yield stress for the  $\langle 110 \rangle / \{111\}$  Pd NWs in Figure 3, where the yield stresses from stage 1 in Figure 2 are plotted with respect to the NW diameters. The yield stress increases as the NW diameters decreases down to 40 nm at which point it reaches a value of 4 GPa, which is an order of magnitude higher than the bulk yield stress. By fitting the yield strength to the standard power-law form  $\sigma_y \propto d^{-n}$ , we obtain  $n \sim 0.61$ , where  $d$  is the NW diameter and  $\sigma_y$  is the yield stress. This  $n$  value falls into the range of 0.5–1, which is typically reported for fcc metals including Al,



**Figure 2.** Stress–strain curves for initially  $\langle 110 \rangle / \{111\}$  Pd NWs with diameters 40–182 nm.



**Figure 3.** Size-dependence of the yield stress for the  $\langle 110 \rangle / \{111\}$  Pd NWs captured from the stage 1 in Figure 2

Cu, Ni, Au, and so forth.<sup>3</sup> The variation of the power law exponent, which is also called the size-dependent exponent, has previously been associated with bulk deformation mechanisms such as dislocation nucleation and dislocation forest cutting. In our study, we have clearly shown that the deformation mechanism in tension is the nucleation of partial dislocations at the vertices (surface) of the rhombic cross section, which propagate across the NW cross section on a  $\{111\}$  slip plane.<sup>23–25</sup> Hence, we show that instead of the strengthening mechanism being that of multiplication or interaction of dislocations as for bulk polycrystalline metals, the stress required to nucleate the partial dislocation from the surface (corresponding to the yield stress) increases by decreasing the NW diameter, which gives the size-dependent exponent  $n \sim 0.61$ . Our power law exponent is indeed similar to the exponent of 0.66 obtained by Zhu et al.,<sup>13</sup> though their Ag NWs were  $\langle 110 \rangle$  wires with a pentagonal cross section and 5-fold twin symmetry. Similar to them, we believe that an increase in the NW stiffness may be one reason for the reduced power law exponent as we also observed an increase in stiffness with decreasing NW diameter as shown in Figure 2.

More importantly, we report, for the first time in Figure 4, a clear size-dependence of the twin propagation behavior, where

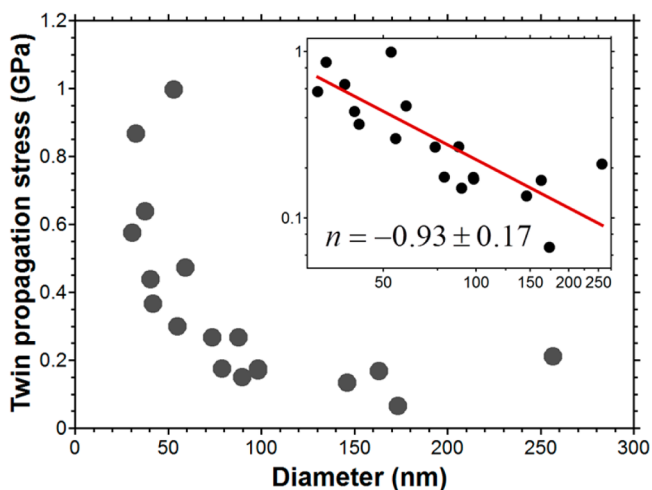


**Figure 4.** Size-dependence of the twin propagation stress during the  $\langle 110 \rangle / \{111\}$  to  $\langle 100 \rangle / \{100\}$  reorientation for Pd NWs captured from the stage 2 in Figure 2

the twin propagation stress was determined by averaging the stress between the strains of 0.1–0.4 in Figure 2. At a critical diameter of about 100 nm, the twin propagation stress begins to increase substantially. Specifically, the twin propagation stress increases nearly 5-fold from about 0.2 GPa to about 1 GPa as the NW diameter decreases from 100 to 30 nm. Furthermore, we find that if the twin propagation stress is analyzed in power-law format, that is,  $\sigma_{tm} \propto d^{-n}$ , where  $\sigma_{tm}$  is the twin propagation stress, the exponent we find is  $n$  close to unity ( $n = 0.93$ ). The  $1/d$  dependence for the twin propagation stress was predicted theoretically but until now has not been observed experimentally before. We explain this exponent value following the micromechanical theory presented by Liang et al.<sup>25</sup> and the surface energy differential model of Li et al.<sup>15</sup> As shown in the Supporting Information, the twin propagation stress can be written as  $\sigma_{tm} = K/d$ , where  $K$  is a geometric factor of the surface reorientation. We have derived the lattice reorientation factor  $K$  for the rhombic single crystalline  $\langle 110 \rangle / \{111\}$  fcc NW as in the surface energy differential model as

$$K = \frac{4\sqrt{3} \left( \gamma_{100} - \frac{\sqrt{3}}{2} \gamma_{111} \right)}{(\sqrt{2} - 1)} \quad (1)$$

We show in Figure 5 a comparison between the analytical surface energy differential model in equation 1 with the twin propagation stress measured experimentally in the present work for three different  $\langle 110 \rangle / \{111\}$  NWs, that is, Au (red stars), Pd (gray solid circles), and AuPd (orange diamonds). We note that the data for the Au and AuPd NWs fall within a narrower size range due to experimental difficulties in synthesizing these NWs with very small and very large diameters. As can be seen, the analytical model with the inverse diameter relationship captures the size-dependent twin propagation stress very accurately, where the slight difference between the model and experiment may be because we ignore the dissipation stress, which is typically less than 100 MPa,<sup>15</sup> possible errors in the surface energy values, or torque caused by grip constraints in the experimental setup, where more detailed discussions are provided in the Supporting Information.

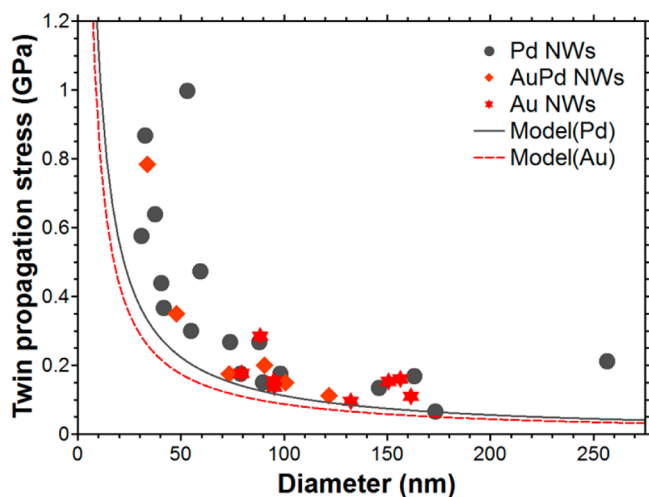


**Figure 5.** Comparison of the analytical surface energy differential model in eq 1 vs experimental data for the twin propagation stress, as measured during the  $\langle 110 \rangle / \{111\}$  to  $\langle 100 \rangle / \{100\}$  reorientation process.

Interestingly, the twin propagation stresses of the AuPd and Au overlap (Figure 5). The similarity of the size-dependence for the three different NWs (Au, Pd, and AuPd) can be explained by the similar difference in surface energies from  $\{111\}$  to  $\{100\}$  that is characteristic of fcc metals.<sup>27,28</sup> The surface energy obtained from GGA calculations for the  $\{111\}$  and  $\{100\}$  surfaces of Pd are 1.92 and 2.33 J/m<sup>2</sup>, while the same surfaces of Au have energies 1.28 and 1.63 J/m<sup>2</sup>, respectively.<sup>28</sup> While the surface energies of Pd are about 50% higher than those of Au for a given orientation, the  $K$  value for Pd (11.16 J/m<sup>2</sup>) is closer ( $\sim 28\%$  difference) to that for Au (8.72 J/m<sup>2</sup>), which results in the similar twin propagation stress at a given diameter as illustrated by the gray solid line and red dotted line in Figure 5. This result shows the validity of our model and also demonstrates the increasing importance of surface energy on the twin propagation stress with decreasing NW diameter. This surface energy differential model predicts a twin propagation stress of around 3.4 GPa for NWs having diameters of 2–5 nm, which is similar to that predicted for metal NWs using MD simulations.<sup>16,17,26</sup> Such high twin propagation stress for NWs with small diameters insinuates the high energy storage application of single crystalline metal NWs using its unique deformation twinning behavior and shape memory properties as proposed in previous simulations.<sup>15–18</sup>

In conclusion, this study clarified the size-dependent twin propagation behavior of metal NWs. The key findings can be summarized as follows: First, for defect-free single crystalline Pd NWs, we observed ultrastrong and ductile behavior as a result of coherent twin propagation regardless of the NW diameter. Second, we clearly showed for the first time that the size-dependent behavior of twin propagation is distinctly different from that of initial yielding, where the inverse proportionality of twin migration stress with diameter (size-dependent exponent  $n \sim 1$ ) can be explained by a surface energy differential model. Finally, we showed that the twin propagation stress increases more dramatically with decreasing NW diameters than the yield stress, demonstrating the fundamental role that surface reorientations play in enhancing the size-dependent mechanical behavior and properties of metal NWs.

Our results also imply the possibility of the energy storage application of single crystalline metal NWs using this unique deformation twinning behavior.

## ■ ASSOCIATED CONTENT

### § Supporting Information

In situ mechanical testing movies showing twin propagation of Pd NW (Movie S1) and force-measurement during tensile test (Movie S2) are provided. The derivation of surface energy differential model (equation 1) and the experimental results of yield strength of Au, Pd, and AuPd NWs are also available. This material is available free of charge via the Internet at <http://pubs.acs.org>.

## ■ AUTHOR INFORMATION

### Corresponding Authors

\*E-mail: (J.P.A.) [jpahn@kist.re.kr](mailto:jpahn@kist.re.kr)

\*E-mail: (B.K.) [bongsoo@kaist.ac.kr](mailto:bongsoo@kaist.ac.kr)

\*E-mail: (I.S.C.) [insukchoi@kist.re.kr](mailto:insukchoi@kist.re.kr)

### Author Contributions

<sup>†</sup>J.-H.S. and H.S.P. contributed equally to this work.

### Notes

The authors declare no competing financial interest.

## ■ ACKNOWLEDGMENTS

This work was supported by KIST R&D program of 2Z03770 (ISC), NSF grant CMMI-1036460 (HSP), NSF DMR-1240933 (JL), Pioneer Research Center Program through NRF funded by the MEST, Korea (2012-0001059), and the Public Welfare & Safety research program through NRF-2012M3A2A1051686.

## ■ REFERENCES

- (1) Park, H. S.; Cai, W.; Espinosa, H. D.; Huang, H. *MRS Bull.* **2009**, *34*, 178–183.
- (2) Greer, J. R.; Hosson, J.; Th, M. D. *Prog. Mater. Sci.* **2011**, *56*, 654–724.
- (3) Kraft, O.; Gruber, P. A.; Mönig, R.; Weygand, D. *Annu. Rev. Mater. Res.* **2010**, *40*, 293–317.
- (4) Weinberger, C. R.; Cai, W. *J. Mater. Chem.* **2012**, *22*, 3277–3292.
- (5) Richter, G.; Hillerich, K.; Gianola, D. S.; Mönig, R.; Kraft, O.; Volkert, C. A. *Nano Lett.* **2009**, *9*, 3048–3052.
- (6) Yoo, Y.; Seo, K.; Han, S.; Varadwaj, K. S. K.; Kim, H. Y.; Ryu, J. H.; Lee, H. M.; Ahn, J. P.; Ihee, H.; Kim, B. *Nano Lett.* **2010**, *10*, 432–438.
- (7) Yoo, Y.; Yoon, I.; Lee, H.; Ahn, J.; Ahn, J. P.; Kim, B. *ACS Nano* **2010**, *4*, 2919–2927.
- (8) Zheng, H.; Cao, A.; Weinberger, C. R.; Huang, J. Y.; Du, K.; Wang, J.; Ma, Y.; Xia, Y.; Mao, S. X. *Nature Commun.* **2010**, *1*, 144.
- (9) Seo, J.-H.; Yoo, Y.; Park, N.-Y.; Yoon, S.-W.; Lee, H.; Han, S.; Lee, S.-W.; Seong, T.-Y.; Lee, S.-C.; Lee, K.-B.; Cha, P.-R.; Park, H. S.; Kim, B.; Ahn, J.-P. *Nano Lett.* **2011**, *11*, 3499–3502.
- (10) Yue, Y.; Liu, P.; Zhang, Z.; Han, X.; Ma, E. *Nano Lett.* **2011**, *11*, 3151–3155.
- (11) Lu, Y.; Song, J.; Huang, J. Y.; Lou, J. *Adv. Funct. Mater.* **2011**, *21*, 3982–3989.
- (12) Sedlmayr, A.; Bitzek, E.; Gianola, D. S.; Richter, G.; Mönig, R.; Kraft, O. *Acta Mater.* **2012**, *60*, 3985–3993.
- (13) Zhu, Y.; Qin, Q.; Xu, F.; Fan, F.; Ding, T.; Zhang, T.; Wiley, B. J.; Wang, Z. L. *Phys. Rev. B* **2012**, *85*, 045443.
- (14) Wu, B.; Heidelberg, A.; Boland, J. J. *Nat. Mater.* **2005**, *4*, 525–529.
- (15) Li, S.; Ding, X.; Li, J.; Ren, X.; Sun, J.; Ma, E. *Nano Lett.* **2010**, *10*, 1774–1779.
- (16) Park, H. S.; Gall, K.; Zimmerman, J. A. *Phys. Rev. Lett.* **2005**, *95*, 255504.

- (17) Liang, W.; Zhou, M. *Nano Lett.* **2005**, *5*, 2039–2043.
- (18) Park, H. S.; Gall, K.; Zimmerman, J. A. *J. Mech. Phys. Solids* **2006**, *54*, 1862–1881.
- (19) Liang, W.; Zhou, M. *Phys. Rev. B* **2006**, *73*, 115409.
- (20) Gall, K.; Sehitoglu, H.; Chumlyakov, Y. I.; Kireeva, I. V. *Acta Mater.* **1999**, *47*, 1203–1217.
- (21) Liu, Y.; Xie, Z.; Van Humbeeck, J.; Delaey, L. *Acta Mater.* **1998**, *46*, 4325–4338.
- (22) Gall, K.; Maier, H. J. *Acta Mater.* **2002**, *50*, 4643–4657.
- (23) Diao, J.; Gall, K.; Dunn, M. L. *Nano Lett.* **2004**, *4*, 1863–1867.
- (24) Park, H. S.; Zimmerman, J. A. *Phys. Rev. B* **2005**, *72*, 054106.
- (25) Leach, A. M.; McDowell, M.; Gall, K. *Adv. Funct. Mater.* **2007**, *17*, 43–53.
- (26) Liang, W.; Srolovitz, D. J.; Zhou, M. *J. Mech. Phys. Solids* **2007**, *55*, 1729–1761.
- (27) Wan, J.; Fan, Y. L.; Gong, D. W.; Shen, S. G.; Fan, X. Q. *Model. Simul. Mater. Sci. Eng.* **1999**, *7*, 189–206.
- (28) Vitos, L.; Ruban, A. V.; Skriver, H. L.; Kollár, J. *Surf. Sci.* **1998**, *411*, 186–202.

Supporting Information

# Origin of size dependency in coherent-twin-propagation mediated tensile deformation of noble metal nanowires

Jong-Hyun Seo,<sup>†,‡,∇</sup> Harold S. Park,<sup>§,∇</sup> Youngdong Yoo,<sup>||</sup> Tae-Yeon Seong,<sup>‡</sup> Ju Li,<sup>¶</sup>

Jae-Pyoung Ahn,<sup>†,\*</sup> Bongsoo Kim,<sup>||,\*</sup> In-Suk Choi<sup>⊥,\*</sup>

<sup>†</sup>Advanced Analysis Center, KIST, Seoul 130-650, Korea

<sup>‡</sup>Department of Materials Science and Engineering, Korea University, Seoul 136-701, Korea

<sup>§</sup>Department of Mechanical Engineering, Boston University, Boston, MA 02215, USA

<sup>||</sup>Department of Chemistry, KAIST, Daejeon 305-701, Korea

<sup>¶</sup>Department of Nuclear Science and Engineering and Department of Materials Science and

Engineering, Massachusetts Institute of Technology, Cambridge, MA 02139, USA

<sup>⊥</sup>High Temperature Energy Materials Research Center, KIST, Seoul 130-650, Korea

KEYWORDS: Nanowires, ultra-strong and ductile, twin propagation, size effect, surface energy

1. After experimentally acquiring the stress-strain curves, we performed a series of additional tensile test with the NW diameter of about 98 nm in the SEM while stopping the test at each deformation stage. Subsequently, we took the NWs at each stage in order to obtain structural details with TEM images in the insets of Figure 1.

**Twin propagation and surface reorientation of the single crystalline Pd NW during stage II :**

The Figure S1 provides more detailed structural information of the inset of Stage 2. As shown in Figure S1 (a), the NW became tilted across the twin boundary. Selected area electron diffraction (SAED) patterns of the original and twinned regions (Figure S1 b,c,d) show that the twin formation reorients the lattice of the NW from  $\langle 110 \rangle$  to  $\langle 100 \rangle$ . The region (b) and (c) indicate single crystallinity of NW during the twin propagation while a concurrent axial reorientation from  $\langle 110 \rangle$  to  $\langle 100 \rangle$  is observed in region (c). The SAED patterns for the region (d) clearly shows the twin boundary structure.

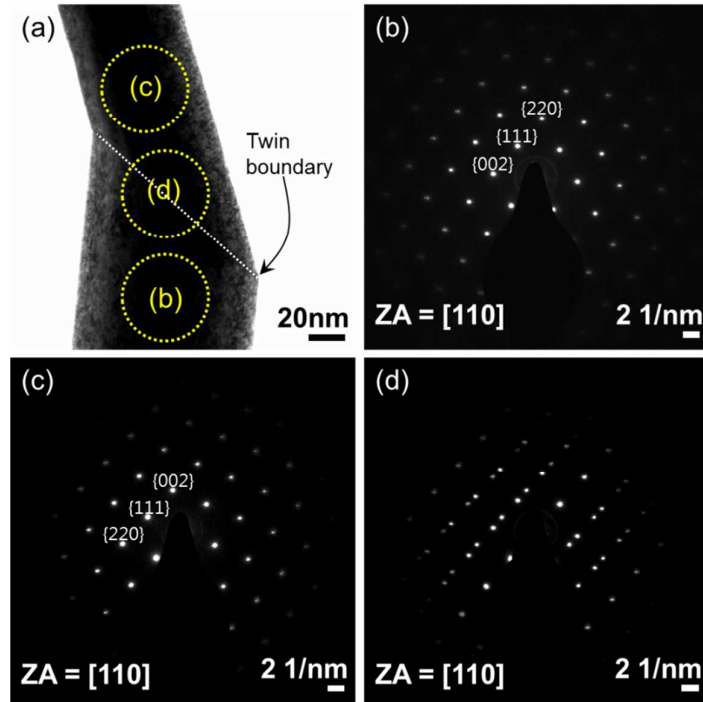


Figure S1: TEM observation at Stage 2 illustrating the geometrical changes that occur during the tensile stress-induced reorientation of the Pd NW from  $\langle 110 \rangle \{111\}$  to  $\langle 100 \rangle \{100\}$ . (a)

Bright field TEM image across the twin boundary (a) and (b,c) SAED patterns acquired from two yellow dotted circles denoted by (b) and (c) with a 180 nm aperture, the NW lattice is changed from an original  $\langle 110 \rangle / \{ 111 \}$  (b) to a twinned  $\langle 100 \rangle / \{ 100 \}$  (c). SAED pattern across the boundary from the circled area (d) shows a clear twin structure.

**2. Derivation of surface energy differential model (equation 12):** As shown in Figure S2, the tensile load induces a lattice reorientation which results in the complete geometrical transformation of the initially  $\langle 110 \rangle \{ 111 \}$  NW into a  $\langle 100 \rangle \{ 100 \}$  NW. The reorientation of the NW results in a change of the cross sectional geometry, from rhombic for the initially  $\langle 110 \rangle \{ 111 \}$  NW to square for the  $\langle 100 \rangle \{ 100 \}$  NW. In conjunction, the cross-sectional area decreases and the four bounding  $\{ 111 \}$  surfaces of the initially rhombic  $\langle 110 \rangle \{ 111 \}$  NW are reoriented to  $\{ 100 \}$  surfaces.

The axial reorientation from  $\langle 110 \rangle$  to  $\langle 100 \rangle$  also results in a significant elongation of the NW, where the change in the NW dimensions can be summarized as

$$d = \frac{2}{\sqrt{6}} \cdot d_0, \quad l = \sqrt{2} \cdot l_0 \quad \dots\dots\dots(1)$$

where  $d_0$  and  $d$  are the initial and final side lengths, respectively, and  $l_0$  and  $l$  are the initial and final axial lengths of the  $\langle 110 \rangle \{ 111 \}$  and  $\langle 100 \rangle \{ 100 \}$  NWs, respectively. Because it is well-known that for metals undergoing plastic deformation, volume is preserved, we could confirm the volume conservation as

$$V_0 = \frac{2\sqrt{2}}{3} d_0^2 \cdot l_0 \quad \dots\dots\dots(2)$$

$$V = d^2 l = \left( \frac{2}{\sqrt{6}} d_0 \right)^2 \sqrt{2} \cdot l_0 = \frac{2\sqrt{2}}{3} d_0^2 \cdot l_0 \quad \dots\dots\dots(3)$$

Work must be done on the NW to propagate the twins that reorient the NW from  $\langle 110 \rangle / \{ 111 \}$  to  $\langle 100 \rangle / \{ 100 \}$ , and so we write the energetics related to twin propagation as

$$\Delta W = \Delta(\gamma S) + \Delta E_{\text{elastic}} + \Delta Q \dots\dots\dots(4)$$

where  $\Delta(\gamma S)$  is the change in surface energy of the four surfaces of the NW due to the lattice reorientation,  $\Delta E_{\text{elastic}}$  is the stored elastic energy and  $\Delta Q$  is the energy dissipation due to the lattice friction, etc. The work done during the tensile testing of the NWs can be written as

$$\Delta W = F \Delta l \dots\dots\dots(5)$$

where  $F$  is the applied force along the NW axis during twin propagation, and  $\Delta l$  is the corresponding length change. Thus, we can calculate the applied force  $F$  by equating (4) and (5) in the following equation (6), where equations (4) and (5) are obtained from Li et al [ref. 1]

$$F = \frac{\Delta(\gamma S)}{\Delta l} + \frac{\Delta E_{\text{elastic}}}{\Delta l} + \frac{\Delta Q}{\Delta l} \dots\dots\dots(6)$$

The elastically stored energy is relaxed during plastic deformation and the dissipation energy is also not a major contribution to the energetics of twin propagation in the NWs, as previously discussed by Li et al. [ref. 1] and Liang et al. [ref. 2]. Thus, we have assumed that the applied force can be written purely in terms of the surface energy difference  $\Delta(\gamma S)$  as a result of the twin migration.

The total surface energies of the  $\langle 110 \rangle / \{ 111 \}$  and  $\langle 100 \rangle / \{ 100 \}$  NWs are written as

$$\gamma S_{\langle 100 \rangle / \{ 100 \} \text{ NW}} = \gamma_{100} \cdot 4l \cdot d \dots\dots\dots(7)$$

$$\gamma S_{\langle 110 \rangle \{111\} NW} = \gamma_{111} \cdot 4l_0 \cdot d_0 = \gamma_{111} \cdot 4\left(\frac{1}{\sqrt{2}}l \cdot \frac{\sqrt{6}}{2}d\right) = \gamma_{111} 4l \cdot d \cdot \frac{\sqrt{3}}{2} \dots \dots \dots (8)$$

where  $\gamma_{111}$  and  $\gamma_{100}$  are the surface energies for the {111} and {100} surfaces, respectively and S is the area of a bounding surface.

The surface energy difference after twin migration can be calculated as

$$\begin{aligned} \Delta(\gamma S) &= \gamma S_{\langle 100 \rangle \{100\} NW} - \gamma S_{\langle 110 \rangle \{111\} NW} \\ &= \gamma_{100} \cdot 4l \cdot d - \gamma_{111} 4l \cdot d \cdot \frac{\sqrt{3}}{2} \\ &= 4l \cdot d \left( \gamma_{100} - \frac{\sqrt{3}}{2} \gamma_{111} \right) \dots \dots \dots (9) \end{aligned}$$

Therefore we can calculate the applied force along the <100> NW direction for twin propagation as

$$F \Delta l = \Delta W = \Delta(\gamma S)$$

The length change is  $\Delta l = (l - l_0) = \frac{(\sqrt{2}-1)}{(\sqrt{2})}l$  so that

$$\begin{aligned} F \cdot \frac{(\sqrt{2}-1)}{\sqrt{2}} \cdot l &= 4d \cdot l \left( \gamma_{100} - \frac{\sqrt{3}}{2} \gamma_{111} \right) \\ F &= 4d \frac{\sqrt{2}}{(\sqrt{2}-1)} \left( \gamma_{100} - \frac{\sqrt{3}}{2} \gamma_{111} \right) \dots \dots \dots (10) \end{aligned}$$

Then, the stress along the reoriented <100> wire can be written as

$$\sigma = \frac{F}{A_{100}} = \frac{F}{d^2} = \frac{4\sqrt{2}}{(\sqrt{2}-1)} \left( \gamma_{100} - \frac{\sqrt{3}}{2} \gamma_{111} \right) \frac{1}{d} \dots \dots \dots (11)$$

where  $A_{100}$  is the cross-sectional area of the reoriented <100> NW with <100>.

Because we measured the diameter  $d_0$  of the  $\langle 110 \rangle / \{ 111 \}$  NWs in our experiment before twin migration, we replace  $d$  with  $d_0$  by inserting  $d = \frac{2}{\sqrt{6}} \cdot d_0$

$$\sigma = \frac{4\sqrt{3}}{(\sqrt{2}-1)} \left( \gamma_{100} - \frac{\sqrt{3}}{2} \gamma_{111} \right) \frac{1}{d_0} \dots\dots\dots(12)$$

Our model given in Equation (12) was plotted with our experimental data in the Figure 5 in the main text. As seen in the main text, the model slightly underpredicts the twin propagation stress, though the overall trend is captured. We believe that one reason for this is because the normal stress in the  $\langle 100 \rangle$  direction may be lower than the apparent stress due to grip constraints at the NW ends.

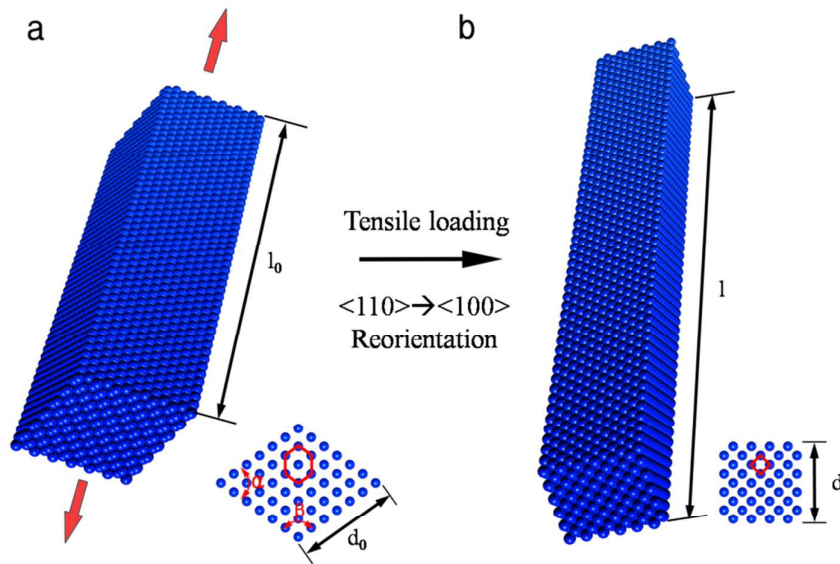


**Figure S2.** Schematic illustrating the geometrical changes that occur during the tensile stress-induced reorientation of the NW from  $\langle 110 \rangle / \{ 111 \}$  to  $\langle 100 \rangle / \{ 100 \}$ .

**3. Size dependence of yield strength:** Unlike the twin migration stress, the size dependence of the yield stress does not overlap for the Pd, AuPd and Au NWs as shown in the Figure S3.

This is because the stacking fault energy is the dominant factor controlling the dislocation nucleation process that governs yielding. Because the stacking fault energy of Pd is about twice that of Au, the yield stress of Pd is higher than Au [ref. 3 ], with the yield stress of AuPd lying in between pure Pd and pure Au.

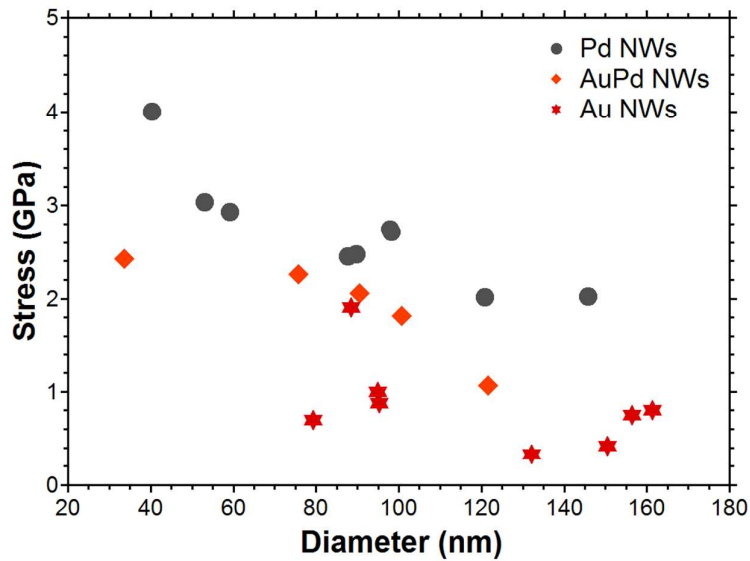
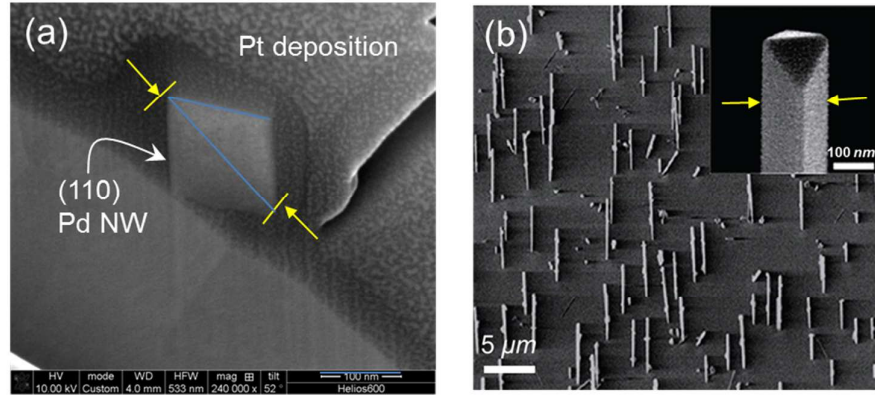


**Figure S3:** Size-dependence of the yield stress for the  $\langle 110 \rangle / \{ 111 \}$  Pd, AuPd, Au NWs.

**4. Calculation of Cross sectional area:** For stress calculation, we divided the force by the rhombic cross-sectional area of the NW. Figure S4 (a) shows that the original NWs with  $\langle 110 \rangle / (111)$  have a rhombic cross-section. We measured the diagonal of the NWs from the side view of the SEM image as in Figure S4 (b) and calculated the area assuming the rhombic area as schematically shown in Figure S4 (c).



(c) Cross-section of Pd NW

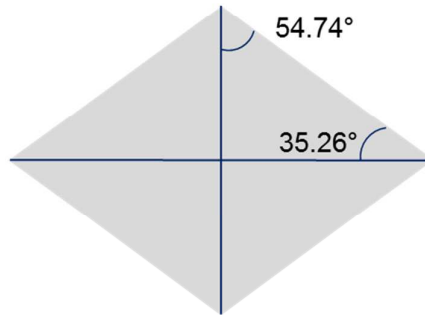


Figure S4: (a) SEM image of the cross-sectional area of a representative Pd NW showing a rhombic shape with  $\langle 110 \rangle \{ 111 \}$ . (b)  $45^\circ$  tilted SEM images of vertically grown Pd NWs on a c-cut sapphire substrate. The inset is a magnified image showing clear facets of the rhombic NW. (c) Schematic of the rhombic cross-section of the Pd NWs based on Figure S4 (a). We used this schematic to calculate the cross-sectional area.

**5. Possible reason for deviation between the measured and predicted twin migration stress in Figure 5 :**

1) Underestimation of the cross sectional area may lead to overestimation of the measured twin propagation stress. As mentioned before, we measured the width of the NWs from the side view of the SEM image. As shown in Figure S5, the diagonal can be underestimated though we tried to calibrate the angle of the view point. However, since we employed the NWs all grown in the same vertical direction, the diagonals were measured in a consistent way so the underestimation should be consistent as well. Hence, the trend and the exponent value should be valid.

2) Possible misalignment of the NW and geometrical tilt during twin propagation may also overestimate the measured stress as well.

3) The dissipation energy (about 100 MPa) was not included in the surface energy differential model as mentioned in the manuscript. This can underestimate the predicted twin migration stress [ref. 1].

4) The predicted twin propagation is quite sensitive to the surface energy values in Eq. (1) in the main text. We used values for surface energy that were obtained from ab initio calculations, but the values can vary depending on the simulation scheme [ref. 3]. Thus, the inaccuracy of the surface energy for (111) and (100) planes we used may deviate and underestimate the predicted twin propagation stress.

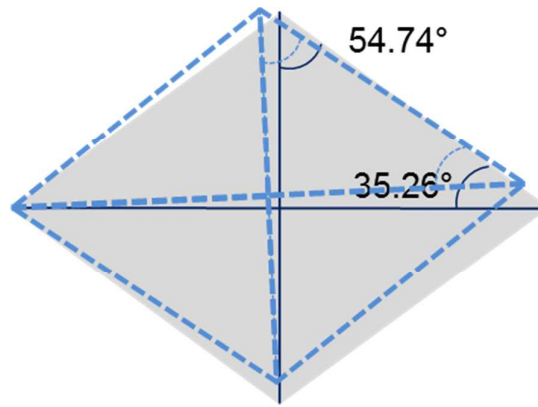


Figure S5: Schematic illustration of possible underestimation of the rhombic cross-section of the Pd NWs.

### References

- [1] S. Li, X. Ding, J. Li, X. Ren, J. Sun, E. Ma, *Nano Lett.* **10**, 1774 (2010).
- [2] W. Liang, D.J. Srolovitz, M. Zhou, *Journal of the Mechanics and Physics of Solids* **55**, 1729 (2007).
- [3] J. Wan, Y.L. Fan, D.W. Gong, S.G. Shen, X.Q. Fan, *Modelling and Simulation in Materials Science and Engineering* **7**, 189 (1999).

## 6. Supplementary movies of *in-situ* tensile testing

We provide two different tensile tests showing in movie S1 and movie S2 to resolve the issue that may arise because of the AFM cantilever. The movie S1 shows the tensile test without the AFM cantilever. The movie S2 shows a tensile test with the AFM cantilever.

Movie S1:

The tensile test without an AFM cantilever showing the twin propagation of a  $\langle 110 \rangle$  Pd NW.

Movie S2:

The tensile test of a  $\langle 100 \rangle$  Pd NW with an AFM cantilever, separated from the  $\langle 110 \rangle$  region remained after the twin propagation was completed.

Both of them showed apparently the same mechanical deformation of the NWs including long range ordered twin propagation behavior. The test in movie S1 is undoubtedly a displacement control controlled by the piezo response of the nanomanipulator. The test in movie S2 may not be an ideal displacement control since the AFM cantilever is attached to the manipulator. However, considering the much higher stiffness of the cantilever and the manipulator than that of the NW, we believe that our AFM cantilever based tensile test is more likely displacement control test by controlling the piezo movement of the manipulator. Furthermore, a significant load drop is explicitly observed, which indicated the displacement control.